Mem. S.A.It. Suppl. Vol. 3, 335

Memorie della
Supplementi

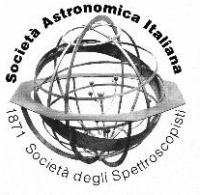

Numerical simulations of astrophysical jets: comparison of integration schemes

S. Massaglia[1], N. Zurlo[1], and G. Bodo[2]

[1] Dipartimento di Fisica Generale, Università di Torino, Via Pietro Giuria 1, I-10125 Torino, Italy
[2] INAF, Osservatorio Astronomico di Torino, Strada dell'Osservatorio 20, I-10025 Pino Torinese (TO), Italy

Abstract. In this paper we model an astrophysical jet and simulate its evolution numerically by means of different numerical schemes, focusing in particular on Godunov-type methods (Roe, HLLE, PPM) but considering also central methods (local Lax-Friedrichs). The results yielded by various codes are then compared, on the basis of various parameters, such as jet morphology, the statistical distributions of basic physical quantities, cocoon features, and the integral value of significant quantities.

Key words. galaxies: jets – hydrodynamics – numerical methods

1. Introduction

Astrophysical jets are certainly among the most spectacular manifestations of stars and galactic nuclei in their youth. These objects have been intensively investigated to understand the basic physical mechanisms that rule their behavior. Different models have been in the last few decades, but it is clear that the basic aspect concerns the presence of a highly collimated outflow of magnetized plasma from a compact object. Furthermore, the analysis of the evolution of this kind of systems requires the solution of the (magneto-)hydrodynamics equations that can be performed analytically only in a few cases. Therefore, the numerical approach to these equations is essential to follow the jet evolution and to compare the results with observations.

Numerical simulations in the field we are dealing with require methods able to handle discontinuities, because of the presence of shocks and shears, so finite volume methods are good candidates to perform well this kind of work. In particular, two general families of finite volume methods are usually implemented: Godunov-type (or upwind) and central methods. But within each family, there is a variety of schemes that differ in spatial reconstruction, temporal accuracy, handling of discontinuities (and in particular, for Godunov methods, and the solution of the Riemann problem).

This is the reason why in the literature one can find several studies using dif-

Send offprint requests to: S. Massaglia
Correspondence to: via Pietro Giuria 1, I-10125 Torino, Italy

ferent codes, at different spatial resolution as well, and it could be very interesting to understand if the differences that often arise between different works derive more from physical effects or from the numerical scheme used to integrate the equations.

It is generally assumed that different numerical methods applied to the same physical problem lead to similar results, but the few works that have investigated this topic (see e.g. Krause & Camenzind 2001) have shown that this assumption is not always correct and, in particular, that there are schemes that are more efficient in the sense that (with the same grid) they can reproduce structures at smaller scales.

In this paper, we aim to contribute clarifying this point, comparing results from four different well known numerical schemes, and also testing the influence of the spatial resolution on the behavior of the simulated jet. In section 2, we present briefly some observations about astrophysical jets. In section 3, we discuss numerical simulation methods we have considered. In section 4, we present the simplified model used to simulate (with different schemes) an astrophysical jet. In section 5, we compare the results obtained from the different numerical schemes. Finally, in section 6, we draw conclusions.

2. Observations of astrophysical jets

Recent multi-wavelength observations of extragalactic jets performed in radio, optical (in particular by HST) and X-ray bands have extended dramatically our knowledge about the complex phenomenology of these objects. By means of these observations, different kinds of objects that can house these jets have been characterized, and at the moment we can classify distinctly these sources as radio galaxies (FR I and FR II), quasars etc. A deeper analysis of these and other related objects led us to the idea of Active Galactic Nucleus (AGN), and in this context a unified model of various types of objects has been proposed (Antonucci 1993, Urry & Padovani 1995).

2.1. Stellar jets

Observations in the optical band and, more recently, at infrared wavelengths indicate the presence of jet-like structures also in galactic giant molecular clouds, regions dominated by star formation, where Young Stellar Objects (YSOs) are found.

Obviously, the spatial extension of this kind of jets (usually not more than some thousands of AU, i.e. a fraction of a parsec) is on a much smaller scale than AGN jets, which are observed to extend continuously from the parsec scale (VLBI) to the kiloparsec scale (VLA), but similar features are still evident. In both cases, the jet ends in a bright, curved structure, usually referred as "hot spot" or "terminal working surface" that delimits the region filled with the material coming from the central object. In both cases, the presence of bright knots along the jet axis is usually interpreted as an indication of strong shocks, caused by the supersonic flow that constitutes the jet. And again in both cases the origin of the jet is presumably corresponding to a compact object: a black hole in the nucleus of a galaxy, for AGN jets, and a young TTaurii star in formation, for YSO jets.

3. Numerical simulation methods

In order to simulate the evolution of an axisymmetric hydrodynamic jet, one deals with a system of hyperbolic conservation equations such as:

$$\frac{\partial q}{\partial t} + \frac{\partial f(q)}{\partial x} = 0 \qquad q = q(x,t) \qquad (1)$$

As we aim to simulate efficiently supersonic flows, in which discontinuities in physical quantities may arise, we need a numerical method able to handle discontinuities (a so-called "shock capturing method"). This is the reason why the authors usually adopt finite-volume schemes. In this kind of scheme, we integrate the equation 1 over a small cell $C_j = [x_{j-\frac{1}{2}}, x_{j+\frac{1}{2}}]$ centered in x_j; then

we define the pointwise value of the corresponding discretized quantity, q_j, as the cell average: $q_j(t) = \int_{x_{j+1/2}}^{x_{j+1/2}} q(x,t)dt$; and finally we calculate the evolution of these quantities by integrating with respect to time, after introducing a small time step Δt:

$$q_j(t+\Delta t) = q_j(t) + \int_t^{t+\Delta t} f(q(x_{j-\frac{1}{2}},t)dt - \int_t^{t+\Delta t} f(q(x_{j+\frac{1}{2}},t)dt \qquad (2)$$

This integration can be performed in different ways, e.g. with a simple Eulerian time step, and the problem is eventually reduced to the evaluation of fluxes at the interface between adjacent cells.

3.1. Central methods

A first, simpler approach to solve the equation 2 is to define the flux at interfaces as the average of fluxes calculated at the centers of adjacent cells. This method, however, reveals to be unstable unless one adds a sufficient amount of numerical viscosity, that leads to the scheme:

$$q_j^{n+1} = \frac{1}{2}\left(q_{j+1}^n + q_{j-1}^n\right) - \frac{\Delta t}{2\Delta x}(f(q_{j+1}^n) - f(q_{j-1}^n)$$

where n denotes the time t and $n+1$ the time $t+\Delta t$.

The result is the well known Lax-Friedrichs (LF) scheme. If we replace $\Delta x/\Delta t$ with the maximum modulus of the eigenvalues (characteristic speeds) at adjacent cells, we obtain a method that is stable as well but with less numerical viscosity, called local-Lax-Friedrichs (LLF).

3.2. Godunov-type methods

In order to calculate the flux at interfaces indicated previously as $f(q(x_{j-\frac{1}{2}}))$, the method proposed by Godunov (1959) is founded on the solution of the Riemann problem, i.e.:

$$\frac{\partial q}{\partial t} + \frac{\partial f(q)}{\partial x} = 0$$

$$q(x,t_0) = \begin{cases} q_l & \text{if } x < x_{j-\frac{1}{2}} \\ q_r & \text{if } x > x_{j-\frac{1}{2}} \end{cases}$$

Because this problem is self-similar, the solution does not depend on time if the CFL number is less than unity (see e.g. Toro 1999 for a full discussion), thus the integration over the time Δt can be easily performed.

The exact solution of the Riemann problem, that for hydrodynamic 1D equations needs the calculations of 3 characteristic directions by solving iteratively a nonlinear algebraic equation, can be also simplified by using approximate Riemann solvers. That is what happens in the Roe method (Roe 1981), in which the corresponding linearized equations are solved, and in HLLE method (Harten et al. 1983; Einfeldt 1988), in which only 2 characteristic directions are considered.

3.3. Higher order extension

The Godunov original method, as well as the Roe and HLLE simplified methods, and also LLF method, are still characterized by a large amount of numerical viscosity, that causes shocks to be smeared over several cells. In order to avoid this drawback, high-order spatial polynomial reconstruction is often used. This is usually put together with a Runge-Kutta time step, aimed at achieving a comparable spatial and temporal accuracy.

Nevertheless, as demonstrated by Godunov (1959), a higher order spatial reconstruction creates spurious oscillations in the solution near shocks and discontinuities. Therefore, one must introduce some kind of control, like slope limiters introduced by Van Leer in his MUSCL approach (Van Leer 1977, 1979) that reduces the order of reconstruction to the first

in cells where are present such features. In that manner the scheme preserves the monotonicity of the solution, acquiring the TVD (total variation diminishing) property even though at the cost of losing the linearity property.

In this paper, we have used LLF, Roe and HLLE methods together with a linear spatial reconstruction (second order in accuracy) and a Monotonized Centered (fully TVD) limiter. On the other hand, we have used also PPM reference code (Colella & Woodward 1984), that includes an exact Godunov solver and a piecewise parabolic spatial reconstruction (third order in accuracy) with more complex controls on the slope to avoid oscillations and with a discontinuity detection mechanism.

4. The jet model

We consider a non-relativistic fluid jet that propagates at supersonic speed in a uniform medium and, at the beginning, is in pressure equilibrium with its environment. Specifically, we make the following assumptions:

- the configuration is and remains axisymmetric
- the fluid has neither viscosity nor thermal conductivity (ideal gas)
- the density of the fluid can vary, according to the equation of state $p/\rho \propto T$; this imply that the specific internal energy is $e=(\gamma-1)p/\rho$, with $\gamma=c_p/c_v$ (in particular, $\gamma=5/3$ for hydrogen)
- magnetics field effects on bulk jet dynamics is negligible, that is equivalent to say that $B^2/8\pi \ll \frac{1}{2}\rho v_{\rm jet}^2$

Under these conditions, the relevant equations are the hydrodynamic equations of mass, momentum and energy conservation:

$$\frac{\partial \rho}{\partial t} + \nabla \cdot (\rho \mathbf{v}) = 0$$

$$\rho \frac{D\mathbf{v}}{Dt} = -\nabla p$$

$$\rho \frac{DE}{Dt} = -\nabla \cdot (p\mathbf{v})$$

where $\frac{D}{Dt} = \frac{\partial}{\partial t} + \mathbf{v} \cdot \nabla$ denotes the Lagrangian (or substantial) derivative.

Because of axisymmetry, using cylindrical coordinates (r, z) such equations can be elaborated in the following conservation form:

$$\frac{\partial}{\partial t}\mathbf{U} + \frac{\partial}{\partial z}\mathbf{F} + \frac{1}{r}\frac{\partial}{\partial r}(r\mathbf{G}) = \mathbf{S}$$

where

$$\mathbf{U} = \begin{pmatrix} \rho \\ \rho v_z \\ \rho v_r \\ E \end{pmatrix}; \quad \mathbf{F} = \begin{pmatrix} \rho v_z \\ p + \rho v_z^2 \\ \rho v_r v_z \\ (E+p)v_z \end{pmatrix};$$

$$\mathbf{G} = \begin{pmatrix} \rho v_r \\ \rho v_z v_r \\ p + \rho v_r^2 \\ (E+p)v_r \end{pmatrix}; \quad \mathbf{S} = \begin{pmatrix} 0 \\ 0 \\ \frac{p}{r} \\ 0 \end{pmatrix}$$

(note that the curved geometry affects only the flux calculation along the radial direction and the introduction of the source term of radial momentum).

This is also the standard form in which equations are integrated numerically, introducing suitable boundary conditions (outflow everywhere except for the injection side) and initial conditions.

4.1. Test case and reference parameters

In order to follow by means of different schemes the temporal evolution of the same physical jet, we have fixed once the relevant physical parameters: in this work we present the results obtained with Mach number $M = v_{\rm jet}/c_{\rm sound,int} = 10$ and density ratio $\nu = \rho_{\rm ext}/\rho_{\rm int} = 3$.

We express lengths in units of the jet initial radius, velocities in units of the initial internal sound speed, and density in units of the initial internal density. Thus our integration domain extends to 40 units in longitudinal direction by 16 units in radial direction. The spatial resolution is determined by a grid of 1024×512 points in the basic test case, that leads to almost square cells.

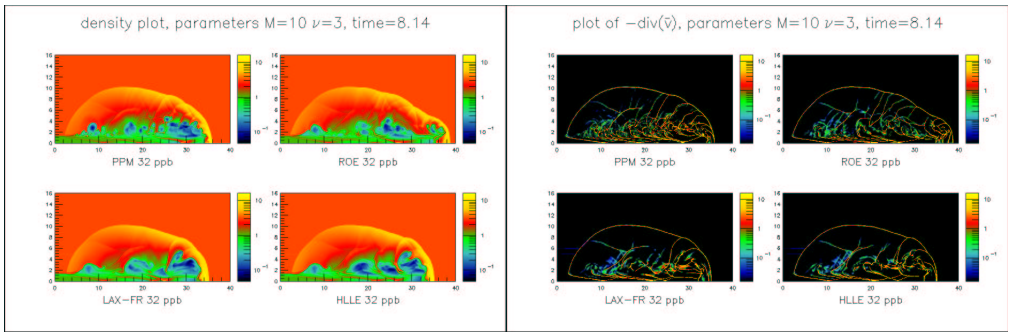

Fig. 1. Left panel:density map. Right panel: map of $(-\nabla \cdot \mathbf{v})$

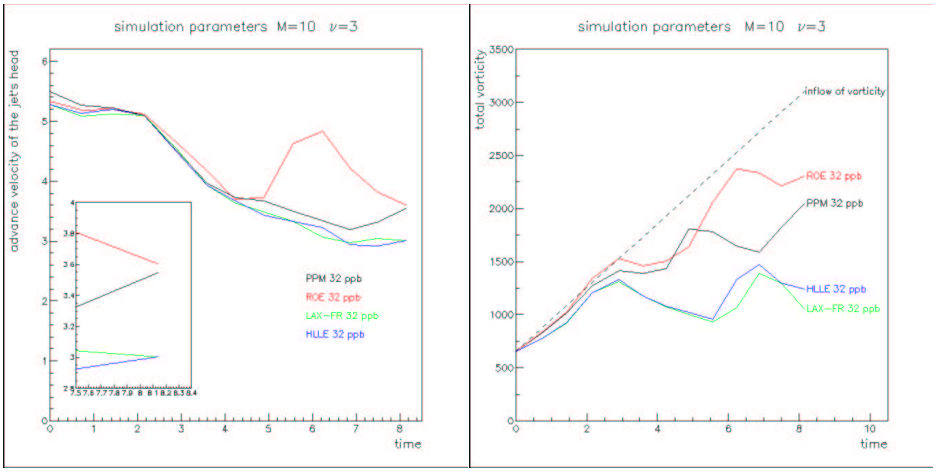

Fig. 2. Velocity of the cocoon head velocity (left panel); temporal evolution of the total vorticity for the different schemes, dashed line shows the vorticity injected with the jet at a constant rate (right panel)

5. Comparison of results

5.1. Morphology

A first way to compare the results yielded by different numerical methods is to show directly the distribution images of basic physical quantities, such as density figure 1 (left panel). Additional information can be obtained representing maps of other interesting quantities, such as the divergence of the velocity field, plotted conventionally with the minus sign $(-\nabla \cdot \mathbf{v})$ in order to have a positive quantity at shocks, that reveals the shock distribution and intensity (figure 1, right panel).

These figures show that the cocoon morphology is essentially the same, but there are sensible differences in particular with respect to small scale structures. Cocoon shapes are quite similar, even though Roe scheme leads to a cocoon more elongated (as we will see in section 5.2 as well). It is evident that PPM produces a higher number of stronger and sharper shocks (and small scale structures in general), while LLF and HLLE produce a lower number of these, smoothing them over adjacent cells and reducing their strength;

Roe scheme seems have an intermediate behavior in terms of number and intensity of shocks.

5.2. Cocoon properties

We have shown that small scale properties may be quite different between various schemes, we investigate now large scale properties, in particular analyzing some cocoon properties, like the cocoon length L_c, the cocoon head velocity v_h, the cocoon maximum radius R_c, the cocoon aspect ratio, defined as R_c/L_c, and the cocoon volume V_c. The cocoon head velocity v_h is plotted in figure 2 (left panel), while other quantities are not plotted because show good agreement between different codes as well.

It is clear that differences are quite small and remain always within a few percent, excepting the case of Roe scheme, that leads to a higher head velocity and, as a consequence, a longer cocoon. This behavior might be correlated to the so-called *carbuncle* phenomenon, pointed out by Quirk (1994), and will require further investigations.

5.3. Integral quantities

We have eventually made comparisons among the various schemes of the temporal evolution integral quantities such as: i) the cocoon thermal and kinetic energy, ii) the ratio of the thermal energy to the injected energy, iii) the ratio of the cocoon thermal energy to the kinetic energy, and iv) the total vorticity. The resulting evolution differences remain inside differences of few percent, at most, but with the exception of the total vorticity that varies considerably, up to about a factor of two among the different schemes (see figure 2, right panel). This can be interpreted by noticing that sources and wells of vorticity depend crucially on the shock curvatures, that are shown to differ among the various schemes (see figure 1, right panel).

6. Conclusions

We have carried out numerical hydrodynamic simulations of supersonic jets using different integration schemes and compared the results. Comparisons have been made at the same spatial resolution and considering the morphology, the characteristics of the cocoon and integral properties of relevant physical quantities. All the schemes examined differ little as far as the large scale properties of the cocoon and integral properties are concerned, with the important exception of the total vorticity that is strictly connected to the details of the morphology of the shock distribution. In fact, we have noted sensible differences in the morphology of shocks among the different schemes examined.

The comparisons have been performed at the same spatial resolution; it remains to be seen whether, increasing the spatial resolution, the different schemes will converge at a certain value and compare the results at that value. This will be discussed in a forthcoming paper.

References

Antonucci, R. 1993, ARA&A 31, 473
Colella, P. & Woodward P.R. 1984, J. Comp. Phys. 54, 174
Einfeldt, B. 1988, Siam J. Numer. Anal. 25, 294
Godunov, S.K. 1959, Mat. Sbornik 47, 271
Harten, A., Lax, P.D., Van Leer, B. 1983, Siam Review 25, 35
Herbig, G.H. 1950, ApJ 111, 11
Krause, M. & Camenzind, M. 2001, A&A 380, 789
Quirk, J.J. 1994, Int. J. Num. Meth. in Fluids 18, 555
Roe, P.L. 1981, J. Comp. Phys. 43, 357
Toro, E.F. 1999, Riemann Solvers and Numerical Methods for Fluid Dynamics, 2nd Edition, Springer-Verlag
Urry, C.M. & Padovani, P. 1995, PASP 107, 803
Van Leer , B. 1977, J. Comp. Phys. 23, 263
Van Leer , B. 1979, J. Comp. Phys. 32, 101